Available online at www.sciencedirect.com
ScienceDirect
Journal of Computational Physics 226 (2007) 1874–1890
JOURNAL OF COMPUTATIONAL PHYSICS
www.elsevier.com/locate/jcp

A compressible magnetohydrodynamic numerical code with time-dependent boundary conditions in cylindrical geometry

Marco Onofri [a,*], Leonardo Primavera [a], Francesco Malara [a], Pasquale Londrillo [b]

[a] *Dipartimento di Fisica, Università della Calabria, ponte P. Bucci, Cubo 31C, 87036 Rende (CS), Italy*
[b] *Osservatorio Astronomico di Bologna, via Ranzani 1, 40127 Bologna, Italy*

Received 26 July 2006; received in revised form 15 June 2007; accepted 18 June 2007
Available online 27 June 2007

Abstract

We describe a numerical code to study the magnetohydrodynamic (MHD) turbulence in a reversed field pinch (RFP) configuration by solving the compressible MHD equations in cylindrical coordinates. The compressibility requires that particular attention should be paid to the boundary conditions to have an accurate control of wave reflections from the boundaries of the computational domain. To fulfill these requirements the boundary conditions are calculated by a decomposition into characteristic waves. We present a method to calculate such boundary conditions in curvilinear coordinates and we apply it to the solution of the MHD equations in cylindrical geometry.

PACS: 52.35.Bj; 52.55.Hc

Keywords: Compressible plasma; Magnetohydrodynamics; Boundary conditions

1. Introduction

Numerical simulations of nonlinear plasma phenomena in experimental devices require the use of cylindrical or toroidal geometry, in which the development of turbulence happens to be different from Cartesian geometry because the majority of the energy exchanges among the modes takes place in the radial and axial directions [1] and the stability properties of the equilibrium are different in Cartesian and cylindrical/toroidal geometries. Moreover, in reversed field pinch (RFP) devices [2], the plasma β (the ratio between the kinetic and magnetic plasma pressure) is rather low (typically $\beta \simeq 10^{-1}$), that means the compressibility effects in the plasma should not be negligible (the incompressible case corresponding to $\beta \to \infty$).

* Corresponding author.
E-mail address: onofri@fis.unical.it (M. Onofri).

0021-9991/$ - see front matter
doi:10.1016/j.jcp.2007.06.015

The numerical solution of the compressible MHD equations presents different difficulties. A first problem is the presence of many more terms in the energy equation, with respect to the incompressible case, which requires long simulation times. Another problem is the choice of boundary conditions. A possible choice, which is commonly used for solving the hydrodynamic equations, are the so-called open boundary conditions [3], which are obtained by analyzing the propagation properties of the simple waves across the boundaries of the numerical domain. This technique has been widely used in Cartesian geometry for fluid flows, but a clear derivation of the conditions for the cylindrical MHD case is missing in the literature, at the best of our knowledge. In this paper, we give a detailed derivation of the method for the cylindrical, MHD case.

Merlin and Biskamp [4] and Cappello and Biskamp [5] studied the development of turbulence in a RFP configuration by solving the MHD equations in cylindrical geometry. However, to avoid the problems that we discussed above, they simplified the equations by assuming constant density (namely incompressibility) and vanishing pressure. This allowed them to avoid both numerical problems coming from compressibility and the solution of the Poisson equation for the pressure (as it is necessary in the incompressible case). The use of such an approach is of course somewhat questionable. However, it has been used until present time [6,7].

In this paper, we solve the fully compressible, nonlinear, MHD equations in both cylindrical and toroidal coordinates. We describe in detail the method used to derive the boundary conditions imposed on density, pressure, velocity and magnetic field. We solve the MHD equations with no approximation of any sort in a fully three-dimensional case. This involves, of course, very long computational times, hence the code has been efficiently parallelized by using MPI directives.

The plan of the paper is the following: in Section 2, we describe the physical domain and the equations that are solved by the code. In Section 3, we describe briefly the numerical techniques used for the spatial and temporal discretizations of the equations. In Section 4, we discuss the boundary conditions, whose derivation is explained in deep detail. The bulk of the calculation is reported in Appendix A. Finally, we present some tests of the numerical code.

2. Equations of the model

To describe a plasma confined in a RFP device, we consider the full set of compressible MHD equations, taking into account viscous (μ), resistive (η) and thermal (k_t) transport coefficients.

The RFP plasma is described by a toroidal geometry with coordinates (r, θ, z), such that:

$$0 \leqslant r \leqslant 1, \quad 0 \leqslant \theta \leqslant 2\pi, \quad z = \xi(r,\theta)R\phi,$$

where $\xi = (1 - \frac{r}{R}\cos\theta)$ is the toroidal shape function, R is the ratio of the major radius to the minor radius of the torus (aspect ratio) and ϕ represents the coordinate along the torus axis. The cylindrical case corresponds to $\xi = 1$. Boundary conditions at the $r = 1$ bounding wall are properly described using a characteristic flux decomposition, while periodicity is assumed in the other two directions (θ and ϕ).

The MHD equations in terms of the field variables density (ρ), momentum components $M_i = \rho v_i$, $M_i = (\rho v_r, \rho v_\theta, \rho v_z)$, magnetic field components $B_i = (B_r, B_\theta, B_z)$ and thermal pressure (p), in dimensionless form, are given by:

$$\frac{\partial \rho}{\partial t} = -\nabla \cdot \mathbf{M}, \tag{1}$$

$$\frac{\partial \mathbf{M}}{\partial t} = -\nabla \cdot \overline{\overline{F}} + \mathbf{J} \times \mathbf{B}, \tag{2}$$

$$\frac{\partial \mathbf{B}}{\partial t} = -\nabla \times \mathbf{E}, \tag{3}$$

$$\frac{\partial p}{\partial t} = -[\nabla \cdot (\mathbf{v}p - k_t \nabla T) + (\gamma - 1)p\nabla \cdot \mathbf{v}] + (\gamma - 1)H_p. \tag{4}$$

In Eq. (4), $\gamma = 5/3$ is the adiabatic index, T is the temperature $T = p/\rho$, and k_t is the thermal conductivity. In the simulations that we describe in this paper k_t has been set to zero assuming that typical values in RFP plas-

mas are very small. Some tests with non-vanishing values of k_t showed that there are no significant differences in the dynamics. The flux tensor $\overline{\overline{F}}$ in Eq. (2) has components

$$F_{ij} = M_i v_j + p\delta_{ij} - \mu\sigma_{ij}, \tag{5}$$

where σ_{ij} is the stress tensor and μ the dimensionless viscosity. In the induction equation (3) the electric field $\mathbf{E}$ is given by the expression:

$$\mathbf{E} = -\mathbf{v} \times \mathbf{B} + \eta\mathbf{J},$$

where $\mathbf{J} = \nabla \times \mathbf{B}$ defines the current density and η is the dimensionless resistivity. In the pressure equation (4), the heat production term H_p is given by:

$$H_p = \eta J^2 + \mu\left[\frac{1}{2}U_{ij}U_{ij} - \frac{2}{3}(\nabla \cdot \mathbf{v})^2\right],$$

where η and μ are the dimensionless resistivity and the viscosity and the tensor U_{ij} is defined as

$$U_{ij} = \sigma_{ij} + \frac{2}{3}(\nabla \cdot \mathbf{v})\delta_{ij}. \tag{6}$$

We use the minor radius a of the torus (or the radius of the cylinder) as the unit length scale to non-dimensionalize the equations. We choose as unit measure for the magnetic field and for the mass density typical values B_0 and ρ_0, respectively, which allows us to define a characteristic value for the Alfvén velocity $v_A = B_0/\sqrt{4\pi\rho_0}$. Hence, we express the velocity in terms of v_A and the time in terms of the typical Alfvén time: $\tau_A = a/v_A$. Finally, the pressure p is measured in units of $\rho_0 v_A^2$.

2.1. MHD equations using toroidal components

The differential line element ds in toroidal geometry is given by:

$$\mathrm{d}s^2 = h_1^2\,\mathrm{d}r^2 + h_2^2\,\mathrm{d}\theta^2 + h_3^2\,\mathrm{d}\phi^2,$$

where

$$h_1 = 1, \quad h_2 = r, \quad h_3 = R\xi(r,\theta),$$

reducing to the usual cylindrical case for $\xi = 1$. Denoting the toroidal derivative by:

$$\frac{\partial}{\partial z} \equiv \frac{1}{R\xi}\frac{\partial}{\partial \phi},$$

the gradient operator components are:

$$\nabla \equiv \left(\frac{\partial}{\partial r}, \frac{1}{R}\frac{\partial}{\partial \theta}, \frac{\partial}{\partial z}\right).$$

while the divergence operator is written as:

$$[\nabla \cdot \mathbf{v}]_t = [\nabla \cdot \mathbf{v}]_c + \frac{v_r\xi_r}{\xi} + \frac{v_\theta\xi_\theta}{r\xi}.$$

Here:

$$\xi_r = -\frac{1}{R}\cos\theta, \quad \xi_\theta = \frac{r}{R}\sin\theta$$

and the term $[\nabla \cdot \mathbf{v}]_c$ is the usual divergence form in cylindrical coordinates:

$$[\nabla \cdot \mathbf{v}]_c = \frac{1}{r}\frac{\partial(rv_r)}{\partial r} + \frac{1}{r}\frac{\partial v_\theta}{\partial \theta} + \frac{\partial v_z}{\partial z}.$$

The curl operator in toroidal coordinates has components:

$$[\nabla \times \mathbf{v}]_r = \frac{1}{r}\frac{\partial v_z}{\partial \theta} - \frac{\partial v_\theta}{\partial z} + \frac{v_z \xi_\theta}{r\xi},$$
$$[\nabla \times \mathbf{v}]_\theta = \frac{\partial v_r}{\partial z} - \frac{\partial v_z}{\partial r} - \frac{v_z \xi_r}{\xi},$$
$$[\nabla \times \mathbf{v}]_z = \frac{1}{r}\frac{\partial (r v_\theta)}{\partial r} - \frac{1}{r}\frac{\partial v_r}{\partial \theta}.$$

In Eq. (2), the flux derivatives $\nabla \cdot \overline{\overline{F}}$ are then expressed in explicit form by:

$$[\nabla \cdot \overline{\overline{F}}]_r = \frac{\partial F_{r,r}}{\partial r} + \frac{1}{r}\frac{\partial F_{r,\theta}}{\partial \theta} + \frac{\partial F_{r,z}}{\partial z} + \frac{(F_{r,r} - F_{\theta,\theta})}{r} + \frac{(F_{r,r} - F_{z,z})\xi_r}{\xi} + \frac{F_{r,\theta}\xi_\theta}{r\xi}$$
$$[\nabla \cdot \overline{\overline{F}}]_\theta = \frac{\partial F_{r,\theta}}{\partial r} + \frac{1}{r}\frac{\partial F_{\theta,\theta}}{\partial \theta} + \frac{\partial F_{\theta,z}}{\partial z} + \frac{2F_{r,\theta}}{r} + \frac{(F_{\theta,\theta} - F_{z,z})\xi_\theta}{r\xi} + \frac{F_{r,\theta}\xi_r}{\xi}$$
$$[\nabla \cdot \overline{\overline{F}}]_z = \frac{\partial F_{r,z}}{\partial r} + \frac{1}{r}\frac{\partial F_{\theta,z}}{\partial \theta} + \frac{\partial F_{z,z}}{\partial z} + \frac{F_{r,z}}{r} + \frac{2F_{\theta,z}\xi_\theta}{r\xi} + \frac{2F_{r,z}\xi_r}{\xi}.$$

Finally, the σ_{ij} viscosity tensor has components:

$$\sigma_{r,r} = 2\frac{\partial v_r}{\partial r} - \frac{2}{3}\nabla \cdot \mathbf{v},$$
$$\sigma_{\theta,\theta} = 2\frac{1}{r}\frac{\partial v_\theta}{\partial r} + 2\frac{v_r}{r} - \frac{2}{3}\nabla \cdot \mathbf{v},$$
$$\sigma_{z,z} = -(\sigma_{r,r} + \sigma_{\theta,\theta}),$$
$$\sigma_{r,\theta} = \sigma_{\theta,r} = \frac{\partial v_\theta}{\partial r} - \frac{v_\theta}{r} + \frac{1}{r}\frac{\partial v_r}{\partial \theta},$$
$$\sigma_{r,z} = \sigma_{z,r} = \frac{\partial v_z}{\partial r} + \frac{\partial v_r}{\partial z} - v_z\frac{\xi_r}{\xi},$$
$$\sigma_{\theta,z} = \sigma_{\theta,z} = \frac{1}{r}\frac{\partial v_z}{\partial \theta} + \frac{\partial v_\theta}{\partial z} - v_z\frac{\xi_\theta}{r\xi}$$

3. Algorithms for space derivatives

Space derivatives are computed using compact finite differences (CFD) along the radial direction r, which allow a high degree of precision in an inhomogeneous system (with respect, for instance, to standard finite difference algorithms) at a moderate operational cost. Note that when small scales are excited, like in a turbulent system, the largest wavenumbers are not perfectly resolved due to the phase errors of the numerical scheme [8]. However the range of well resolved scales is much larger than with ordinary finite differences. Along the two other coordinates (θ and ϕ), we exploit the natural periodicity of the problem and we use fast Fourier transform (FFTs) algorithms. Finally, time integration is given by a third-order Runge–Kutta explicit scheme.

3.1. Pseudo-spectral algorithm for periodic coordinates

The code evaluates the spatial derivatives for the periodic angular coordinates (θ, ϕ) by transforming the quantities in the spectral Fourier space. This is realized first by introducing the uniform grids:

$$\theta_k = \Delta_\theta k, \quad k = 0, 1, \ldots, N_\theta - 1, \quad \Delta_\theta = \frac{2\pi}{N_\theta},$$
$$\phi_l = \Delta_\phi l, \quad l = 0, 1, \ldots, N_\phi - 1, \quad \Delta_\phi = \frac{2\pi}{N_\phi},$$

N_θ and N_ϕ being the number of grid points in the azimuthal and axial directions, respectively. Then the quantities are transformed in the spectral space by using discrete fast Fourier transforms, alternatively in

the θ or ϕ directions, according to the variable whose derivative has to be computed. Finally, the quantities are multiplied by the appropriate wavenumber and transformed back to the physical space. In practice the program works in the physical space, transforming the quantities in the spectral space only when a derivative with respect to θ or ϕ has to be computed. This allows to save CPU time: (a) the number of nonlinear terms in the equations is higher than the number of derivatives to calculate; (b) the spatial derivatives in the radial direction are computed directly in the physical space. Furthermore, by using this technique, we do not need to use two-dimensional FFTs, which decreases the total amount of memory needed by the code. In fact, when using two-dimensional FFTs one needs, to save CPU time, to compute the derivatives in the two directions simultaneously and to store these intermediate values if they are not immediately used. This involves a much larger use of computer memory with respect to our case. The pseudo-spectral scheme is not de-aliased.

As usual, for any variable $f(\theta_k, \phi_l)$ we denote with $\hat{f}_m(\phi_l)$ the real-to-complex θ-transformed variable

$$\hat{f}_m(\phi_l) = \frac{1}{N_\theta} \sum_{k=0}^{N_\theta - 1} f(\theta_k, \phi_l) \mathrm{e}^{-\mathrm{i}m\theta_k}, \quad m = 0, 1, \ldots, N_\theta/2,$$

where $\hat{f}_{-m} = \hat{f}_m^*$, and with $\hat{f}_{m,n}$ the complex-to-complex ϕ-transformed variable

$$\hat{f}_{m,n} = \frac{1}{N_\phi} \sum_{l=0}^{N_\phi - 1} \hat{f}_m(\phi_l) \mathrm{e}^{-\mathrm{i}n\phi_l}, \quad n = 0, 1, \ldots, N_\phi/2,$$

with the reality condition $\hat{f}_{-m,-n} = \hat{f}_{m,n}^*$.

3.2. Compact FD algorithms for the radial coordinate

For the radial coordinate we use compact finite difference algorithms [8] to compute the derivatives. Over the interval $0 \leqslant r \leqslant 1$ we can choose either a uniform grid spacing of length N_r

$$r_j = \Delta_r(j + 1/2), \quad j = 0, 1, \ldots, N_r, \quad \Delta_r = \frac{1}{N_r + 1/2}$$

or a nonuniform grid $r(x)$ of the form

$$r_j = L \sin(x_j/2), \quad x_j = \Delta_x(j + 1/2), \quad j = 0, 1, \ldots, N_r, \quad \Delta_x = \frac{\pi}{N_r + 1/2},$$

where L is a normalization scale defined by the condition $r_{N_r} = 1$. The spacing between grid points decreases when approaching $r = 1$, in order to enhance spatial resolution close to the physical boundary of the torus, where we expect the majority of the dynamical phenomena happen. In both cases, the $r = 0$ point is avoided by taking a staggered grid spacing. Therefore, the regularity conditions around the $r = 0$ point are defined by noticing that f_0 labels the value at $r = \Delta_r/2$ and

$$f_{-j} = \pm f_{j-1}, \quad j = 1, 2, \ldots \tag{7}$$

for even (odd) functions $f(r)$. Parity conditions for field variables are given in terms of the θ-transformed components $\hat{f}_m(r)$, in the following way [9]:

- *even functions* are even for even $m = 0, 2, \ldots$ and odd for odd $m = 1, 3, \ldots$
- the reverse condition holds for *odd functions*.

The MHD field variables satisfy the parity conditions:

(1) scalars (ρ, p) and axial vector components (v_z, B_z) are *even functions*,
(2) radial and poloidal vector components $(v_r, v_\theta, B_r, B_\theta)$ are *odd functions*.

In the case of the nonuniform grid the radial derivatives are computed as an x derivative:

$$\frac{\mathrm{d}}{\mathrm{d}r} = J(x)^{-1}\frac{\mathrm{d}}{\mathrm{d}x}, \quad J(x) = \frac{\mathrm{d}r}{\mathrm{d}x} = \frac{L}{2}\cos(x/2).$$

Since the Jacobian function is an even function, parity conditions for $f(r)$ carry over unchanged for $f(x)$ when $r \to x$.

To compute the r (or x) derivative $Df \equiv f'(x)$, we use forth-order accurate compact finite difference schemes given by the implicit system

$$[Df]_{j-1} + 4[Df]_j + [Df]_{j+1} = \frac{3}{\Delta}[f_{j+1} - f_{j-1}],$$

at the interior points $j = 0, 1, \ldots, N_r - 1$ and the second-order scheme

$$2[Df]_{j-1} + [Df]_j = \frac{1}{2\Delta}[5f_j - 4f_{j-1} - f_{j-2}],$$

at the $j = N_r$ boundary point. Due to the fact that the matrix inversion is a global operation, the higher numerical error at the boundary propagates to the interior points. However, we checked that when the resolution is sufficiently high, the theoretical precision far from the boundary is recovered. Note that the $j = 0$ point is an interior point and $j = -1$ values are then provided by the parity conditions. Since the code is 3D and compressible, the demands in terms of CPU time and storage are quite severe. To improve the performances and lower the memory storage, the code has been parallelized by using MPI directives. We parallelized the code along the z direction: the computational domain is divided in equal sub-domains along z and each of them is assigned to a processor. Unfortunately, the speed up in CPU times is limited from the fact that parallel FFT procedures do not perform well in one dimension, due to the excess of communications needed to transfer data among the processors.

4. Boundary conditions

Boundary conditions can be of two types: (a) *physical boundary conditions*, imposed by the nature of the problem under study, and (b) *numeric boundary conditions*, necessary to make the problem numerically well-posed. The physical conditions are imposed by the problem that must be solved, but they may not be sufficient to solve the problem numerically. The number of necessary and sufficient boundary conditions can be less than the number of primitive variables. In these cases, even if the physical boundaries make the mathematical problem well-posed, then the numerical problem may be ill-posed due to the discretization of the computational domain [10]. If this is the case it is necessary to specify numerical boundary conditions in addition to the physical ones. The numerical boundaries can be considered as compatibility relations that avoid the uncertainty in the variables that are not specified by the physical conditions and they prevent numerical effects like wave reflections from a nonreflecting boundary. Usually, in the incompressible case, the physical boundary conditions are sufficient to provide enough conditions for all the physical quantities, except the pressure, which must be calculated to guarantee the solenoidality of the velocity field [11]. On the contrary, in the compressible case the pressure does not depend on the velocity field and additional boundary conditions must be specified for the density and the pressure (or temperature).

The method used to calculate the numerical boundary conditions is based on a local one-dimensional inviscid (LODI) set of equations written at the boundary in characteristic form [3]. Let us consider a hyperbolic set of equations in the following form:

$$\frac{\partial \mathbf{U}}{\partial t} + \mathbf{A}\frac{\partial \mathbf{U}}{\partial x} = 0, \tag{8}$$

where $\mathbf{U}(x,t)$ is an n-component vector and $\mathbf{A}$ is an $n \times n$ matrix. We look for solutions of the form:

$$\mathbf{U} = \mathbf{U}(x - ct),$$

which are waves that propagate in the x direction with speed c. If we define

$$\xi = x - ct$$

we can write Eq. (8) in the following form:

$$\mathbf{A}\frac{\partial \mathbf{U}}{\partial \xi} = c\frac{\partial \mathbf{U}}{\partial \xi}. \tag{9}$$

Hence the velocities of the waves are the eigenvalues of the matrix A, which can be calculated by imposing the following condition:

$$|\mathbf{A} - c\mathbf{I}| = 0,$$

where $\mathbf{I}$ is the unit matrix.

For each eigenvalue c we can calculate an eigenvector $\mathbf{W}_c$ by solving the system (9). A generic vector that is solution of the system (8) can be written as a linear combination of the eigenvectors:

$$\frac{\partial \mathbf{U}}{\partial \xi} = \sum_c L_c \mathbf{W}_c.$$

The eigenvalues can be both positive and negative, which means that the equations describe both incoming and outgoing waves. The time derivative of the vector $\mathbf{U}$ at the boundary has a contribution from incoming waves and a contribution from outgoing waves:

$$\frac{\partial \mathbf{U}}{\partial t} = \left(\frac{\partial \mathbf{U}}{\partial t}\right)_{\text{in}} + \left(\frac{\partial \mathbf{U}}{\partial t}\right)_{\text{out}}.$$

The outgoing part $(\partial \mathbf{U}/\partial t)_{\text{out}}$ can be evaluated from internal points, which, on the other hand, do not give any information about the incoming contribution $(\partial \mathbf{U}/\partial t)_{\text{in}}$. The physical boundary conditions give the possibility of finding a relation between the amplitudes of the incoming waves and the amplitudes of the outgoing waves, so that the incoming waves can be expressed as a function of the outgoing waves.

The characteristic boundary conditions have usually been calculated for hydrodynamical problems in Cartesian coordinates. Here we calculate them for MHD equations in cylindrical coordinates. The extension to the toroidal case is straightforward, though more complicated from the point of view of computational details.

In the problem that we want to study, at the point $r = 1$, the plasma is assumed to be bounded by a solid, viscous, wall acting as a perfect conductor, which leads to the following physical conditions:

$$B_r(r = 1) = 0,$$
$$v_r(r = 1) = 0,$$
$$v_\theta(r = 1) = 0,$$
$$v_\phi(r = 1) = 0.$$

The first condition means that the magnetic field cannot penetrate the wall (perfect conductor) and the last three conditions are due to the presence of a finite viscosity at the wall, imposing that the fluid and the wall travel at the same (vanishing, in this case) speed. The boundary values for the other variables $(B_\theta, B_\phi, \rho, p)$ have to be derived using a characteristic decomposition method.

For that purpose, we consider the contributions to the time derivatives coming from the radial derivatives of the ideal terms. The Reynolds numbers are considered to be high enough that the dissipative terms can be viewed as corrections to be applied separately. The ideal MHD equations can be written in the form of conservation laws of the kind expressed by Eq. (8). To solve this system of equations it is necessary to choose a coordinate system. Even though the vector $\mathbf{U}$ satisfies the conservation law, its individual components are not necessarily conserved in a given coordinate system. This is the case of the cylindrical coordinates, where a source term is present due to the geometry. If we write the equations using the covariant components of the vectors, the equations take the form of conservation laws with the addition of geometric source terms, where the vector $\mathbf{U}$ is:

$$\mathbf{U} = (\rho, v_r, rv_\theta, v_z, B_r, rB_\theta, B_z, p).$$

A technique to extend the wave propagation method to curvilinear geometry is to convert the equations in locally valid orthonormal bases, solve the resulting Cartesian problems and then apply a deorthonormalization [12]. However, in our case the source terms vanish due to the physical boundary conditions that we have chosen, so that the characteristic decomposition can be done as in the Cartesian case, but with a different vector of unknown variables, containing the covariant components of the velocity and magnetic field. The results obtained with this procedure can be used for the MHD equations every time the source terms are zero, which depends on the choice of physical boundary conditions.

Following the procedure described above, we find the velocities of the waves that can propagate in the radial direction and write the time derivative at the boundary for all the physical quantities as linear combinations of the wave amplitudes (the details of the calculations are reported in Appendix A). The LODI equations at the boundary, with conditions $v_r = v_\theta = v_z = B_r = 0$, are

$$\frac{\partial \rho}{\partial t} = -\frac{c_\mathrm{f}}{c_T^2}(L_\mathrm{f}^+ - L_\mathrm{f}^-), \tag{10}$$

$$\frac{\partial v_r}{\partial t} = -\frac{c_\mathrm{f}^2}{\gamma p}(L_\mathrm{f}^+ + L_\mathrm{f}^-), \tag{11}$$

$$\frac{\partial (rB_\theta)}{\partial t} = -rB_\theta \frac{c_\mathrm{f}}{\gamma p}(L_\mathrm{f}^+ - L_\mathrm{f}^-), \tag{12}$$

$$\frac{\partial B_z}{\partial t} = -B_z \frac{c_\mathrm{f}}{\gamma p}(L_\mathrm{f}^+ - L_\mathrm{f}^-), \tag{13}$$

$$\frac{\partial p}{\partial t} = -c_\mathrm{f}(L_\mathrm{f}^+ - L_\mathrm{f}^-), \tag{14}$$

where L_f^+ and L_f^- are the amplitudes of the outgoing and incoming fast magnetosonic waves, respectively, c_f is their velocity and c_T is the sound speed. The fact that the only waves that give a contribution to the time derivatives at the boundary are the magnetosonic fast waves could have been expected. In fact, since the velocity and the magnetic field radial components are both vanishing at the boundary, the only propagating mode that could cross the boundary is the fast magnetosonic wave.

The incoming waves depend on the solution out of the computational domain and cannot be calculated from the interior points. Hence the incoming wave's amplitude L_f^- must be expressed in terms of the outgoing wave's amplitude L_f^+ [3,13]. The condition $v_r = 0$ implies:

$$L_\mathrm{f}^- = -L_\mathrm{f}^+,$$

which is a condition of reflection for the fast magnetosonic waves at the boundary. Finally, the amplitude of the outgoing wave can be expressed in terms of the radial derivatives of the physical quantities calculated from the interior points:

$$L_\mathrm{f}^+ = \frac{c_T^2}{2c_\mathrm{f}^2}\left(B_\theta \frac{1}{r}\frac{\partial (rB_\theta)}{\partial r} + B_z \frac{\partial B_z}{\partial r} + \frac{\partial p}{\partial r} + \rho c_\mathrm{f} \frac{\partial v_r}{\partial r}\right). \tag{15}$$

The time evolution at the boundary for ρ, B_θ, B_z and p is given by Eqs. ((10), (12)–(14)) , where L_f^+ is given by Eq. (15), with the addition of all the terms of the original Eqs. (1)–(4) that have not been included in the characteristic analysis, which contain derivatives with respect to θ and z and the dissipative terms. In addition, the physical boundary conditions $v_r = v_\theta = v_z = B_r = 0$ are imposed. The characteristic boundary conditions have been calculated for the ideal equations. In the non-ideal case, when viscosity and resistivity are present in the plasma, additional physical boundary conditions may be necessary.

Poinsot and Lele [3] have tested several viscous boundary conditions for different sets of ideal boundary conditions. When the velocity is imposed on the boundary they found that a good choice is to impose that the normal stress is constant along the normal to the boundary. In our case, in cylindrical coordinates, this condition corresponds to: $[\nabla \cdot \bar{\bar{\sigma}}]_r = 0$. Moreover, due to the presence of resistivity, additional conditions must be imposed on the magnetic field. On a conducting wall the electric field has vanishing parallel components, and the same condition must hold in the plasma at the boundary because the parallel components of the electric field are continuous crossing the wall. At the plasma boundaries $\mathbf{v} = 0$, so the electric field is given by

$\mathbf{E} = \eta\mathbf{J} = \eta\nabla \times \mathbf{B}$, and the condition of vanishing parallel electric field implies $J_y = J_z = 0$. Therefore we impose vanishing poloidal and toroidal currents at the boundary, which ensures the continuity of the electric field across the boundary. The boundary condition $J_z = 0$ is not imposed for the (0,0) mode. In fact, to obtain plasma relaxation with a field reversal, the system must be driven from the outside. This is realized assuming a constant toroidal current, which is equivalent to impose a constant poloidal magnetic field at the boundary for the (0,0) mode [14–17].

5. Setup of the initial conditions

In order to test the numerical code we checked the conservation of energy and applied it to a simplified case that has been studied previously [4]. A reversed field pinch is a toroidal configuration used to confine plasmas in fusion machines [18–20]. The poloidal and toroidal components of the magnetic field in an RFP are mostly generated by electric currents flowing in the plasma and they are of the same order of magnitude. This configuration is characterized by a safety factor $q = rB_\phi/RB_\theta$ which is less than unity in the core and negative at the edge, and the toroidal magnetic field changes sign at the edge with respect to the core. Due to this shape of the safety factor many $m = 1$ and $n > R/a$ modes are resonant in the plasma, while the B_ϕ reversal surface is resonant for all $m = 0$ modes [2] (we remind the reader that a is the torus minor radius and R is the major radius).

In a typical RFP experiment the discharge is generated by inducing a strong toroidal current in an ionized plasma with a weak, initially homogeneous toroidal magnetic field B_0, corresponding to the toroidal flux $\psi_t = \pi a^2 B_0$. In the initial phase the discharge is rather turbulent, since the configuration is highly unstable. Such turbulent states are expected to show self-organization [1]. It has been observed that, no matter what the initial conditions are, the reversed field pinch configuration is reached spontaneously and maintained in time against resistive diffusion with enough applied toroidal voltage [21–23]. The plasma provides the conversion of the supplied poloidal magnetic flux into toroidal magnetic flux through a dynamo mechanism. This evidence has led to the formulation of plasma relaxation theory by Taylor [24], who conjectured that the self-organization is reached by decay of the energy W under the constraint of constant magnetic helicity. The result of this relaxation is a force-free magnetic field.

As the initial state in this simulation a force-free equilibrium magnetic field has been chosen, characterized by the following safety factor [25]:

$$q(r) = 0.4(1 - 1.8748r^2 + 0.83232r^4), \tag{16}$$

which is obtained by resistive diffusion from a stable configuration [26]. The magnetic field can be calculated from the safety factor and from the force-free condition:

$$\mathbf{J} \times \mathbf{B} = \mathbf{0}. \tag{17}$$

By looking for solutions of the form:

$$B_\theta = B_\theta(r),$$
$$B_z = B_z(r).$$

Only the r component of Eq. (17) is not identically zero and it becomes:

$$\frac{\mathrm{d}}{\mathrm{d}r}\left(\frac{B_\theta^2 + B_z^2}{2}\right) + \frac{B_\theta^2}{r} = 0. \tag{18}$$

We can express B_z in terms of the safety factor q:

$$B_z = \frac{qB_\theta}{r} \tag{19}$$

and Eq. (18) can be written as:

$$\frac{\mathrm{d}}{\mathrm{d}r}\left[B_\theta^2\left(\frac{q^2 + r^2}{2r^2}\right)\right] + \frac{B_\theta^2}{r} = 0.$$

The above equation can also be put in the following form:

$$\frac{q^2+r^2}{2r^2}\frac{\mathrm{d}B_\theta^2}{\mathrm{d}r}+B_\theta^2\left[\frac{1}{r}+\frac{\mathrm{d}}{\mathrm{d}r}\left(\frac{q^2+r^2}{r^2}\right)\right]=0$$

which can be solved for B_θ:

$$B_\theta^2=B_{\theta_0}^2\exp\left\{-\int\frac{2r^2}{q^2+r^2}\left[\frac{1}{r}+\frac{\mathrm{d}}{\mathrm{d}r}\left(\frac{q^2+r^2}{r^2}\right)\right]\mathrm{d}r\right\}$$

whilst B_z can be obtained from Eq. (19). This equilibrium is strongly unstable with respect to the $(m=1,n=-2)$ mode, therefore the following perturbation has been superposed to the equilibrium field:

$$v_r=\epsilon(1-r^2)(\cos(\theta-2z/R)+\cos(\theta-z/R)), \tag{20}$$

$$v_\theta=\epsilon(1-r^2)(\sin(\theta-2z/R)+\sin(\theta-z/R)). \tag{21}$$

The r dependence has been chosen to be compatible with the boundary conditions (v_r and v_θ must be even functions of r for the $m=1$ mode and they must vanish at the boundary) ϵ is the amplitude of the perturbation, which has been set to $\epsilon=10^{-4}$, namely we start with a linear perturbation.

The boundary condition imposed on the mean poloidal magnetic field ($B_\theta(a)=\text{const.}$) corresponds to the constancy of the total toroidal current I:

$$I=\int_S\mathbf{J}\cdot\hat{\mathbf{n}}\,\mathrm{d}s=\int_S(\nabla\times\mathbf{B})\cdot\hat{\mathbf{n}}\,\mathrm{d}s=\int\mathbf{B}\cdot\mathrm{d}\mathbf{l}=\int B_\theta(a)a\,\mathrm{d}\theta=2\pi a\overline{B}_\theta.$$

The axial magnetic flux ψ_t is also conserved due to the boundary conditions, as can be seen from Eq. (3):

$$\frac{\mathrm{d}\psi_\mathrm{t}}{\mathrm{d}t}=-\int_S(\nabla\times\mathbf{E})\cdot\hat{\mathbf{n}}\,\mathrm{d}s=-\int\mathbf{E}\cdot d\mathbf{l}=-\int E_\theta(a)a\,\mathrm{d}\theta=-2\pi a\bar{E}_\theta.$$

Since $\mathbf{E}=\eta\mathbf{J}-\mathbf{v}\times\mathbf{B}$, from the conditions $J_\theta=\mathbf{v}=0$ at the boundary, it follows that $\mathrm{d}\psi_\mathrm{t}/\mathrm{d}t=0$. This means that the average of the axial field over the plasma cross-section $\langle B_z\rangle=\psi_\mathrm{t}/\pi a^2$ is also constant in time. Therefore, the pinch parameter:

$$\Theta=\frac{aI}{2\psi_\mathrm{t}}$$

(namely the toroidal current normalized to the axial magnetic flux) must remain constant in time, while in general the field reversal parameter:

$$F=\frac{B_z^{0,0}(a)}{\langle B_z\rangle}$$

(representing the normalized toroidal field at the boundary) will show a temporal dependence. These boundary conditions make the system strongly driven from the outside since there is a continuous input of electromagnetic energy. In fact the Poynting vector at $r=a$, for the mean fields (the $(0,0)$ mode) can be written as:

$$\mathbf{E}^{0,0}\times\mathbf{B}^{0,0}=-\hat{\mathbf{r}}E_z^{0,0}B_\theta^{0,0}=-\hat{\mathbf{r}}\eta\frac{B_\theta^{0,0}}{r}\frac{\partial(rB_\theta^{0,0})}{\partial r}.$$

The other two components of the Poynting vector are vanishing at the boundary because $J_\theta=J_r=0$ and $\mathbf{v}=0$. The dynamo action is demonstrated if the reversal of the axial field ($F<0$) is maintained. This cannot be obtained in a purely axisymmetric situation, but it requires the presence of modes $(m,n)\neq(0,0)$ in the spectrum. If only the mean field is present, its temporal evolution shows the loss of the initial reversal and a steady state is produced, without any reversal.

As a first test the conservation of energy has been checked. By multiplying Eq. (2) by $\mathbf{v}$ and Eq. (3) by $\mathbf{B}$, we obtain the following energy balance equation:

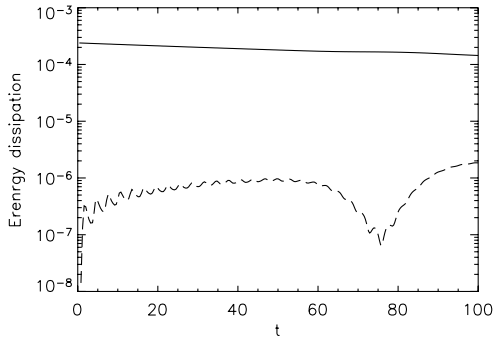

Fig. 1. Energy conservation: the physical dissipation (solid line) is much larger than the numerical dissipation (dashed line).

$$\frac{\partial}{\partial t}\left(\frac{1}{2}B^2+\frac{1}{2}\rho v^2\right)+\nabla\cdot\left[\mathbf{v}\left(\frac{1}{2}\rho v^2+p\right)-(\mathbf{v}\times\mathbf{B})\times\mathbf{B}-\eta\mathbf{B}\times(\nabla\times\mathbf{B})+\mu(\bar{\bar{\sigma}}\cdot\mathbf{v})\right]$$
$$-p\nabla\cdot\mathbf{v}+\eta(\nabla\times\mathbf{B})^2+\mu(\bar{\bar{\sigma}}\cdot\nabla)\mathbf{v}=0. \tag{22}$$

The first term in Eq. (22) is the time derivative of kinetic and magnetic energy, the terms in square brackets represent the flux of energy through the boundary, the term $p\nabla\cdot\mathbf{V}$ is the work of pressure forces and the last two terms represent the energy dissipation due to the viscosity and the resistivity. Note that the last two terms are equal to the heat production term H_p in Eq. (4). Integrating Eq. (22) over the computational domain we obtain the following equation:

$$\int_V\frac{\partial}{\partial t}\left(\frac{1}{2}B^2+\frac{1}{2}\rho V^2\right)\mathrm{d}^3\mathbf{r}-\int_S\eta\frac{B_\theta}{r}\frac{\partial(rB_\theta)}{\partial r}\,\mathrm{d}S+\int_V p\,\nabla\cdot\mathbf{V}\,\mathrm{d}^3\mathbf{r}+\int_V\left[\eta(\nabla\times\mathbf{B})^2+\mu(\bar{\bar{\sigma}}\cdot\nabla)\mathbf{V}\right]\mathrm{d}^3\mathbf{r}=0 \tag{23}$$

The surface integral is the radial component of the Poynting vector, which represents the injection of energy into the system.

The analytical relation (23) is not exactly satisfied numerically due to truncation errors introduced by the discretization in space and time. We define "*numerical dissipation*" the non-vanishing value of the left-hand side of Eq. (23) evaluated numerically. To assess the importance of the truncation induced by the numerical scheme, one can compare this quantity with the physical dissipation, namely with the loss of energy due to the physical viscosity and resistivity (the last integral in Eq. (23)). In Fig. 1 it is shown that the energy dissipated by physical mechanisms is much larger than the energy dissipated by numerical effects, therefore the energy balance equation (23) is well satisfied.

6. Results

Although the code works both in cylindrical and toroidal geometry, up to now we started by studying only the cylindrical case, carrying out a series of runs, to analyze the differences with previous works, which use the same geometry.

A first run (Run 1) has been performed with simplified equations to verify that the reversal of the magnetic field is obtained in the case, studied in previous works [4], where the density ρ is assumed to be constant in space and time and the pressure p is assumed to be vanishing. There is an inconsistency in this approximation. In fact it gives an inward velocity $V_r^{0,0}<0$, which requires $\nabla\cdot\mathbf{V}\neq 0$, and the density following the continuity equation would not remain homogeneous, but would become more concentrated in the center.

The viscosity and resistivity used in the run are $\mu=10^{-4}$, $\eta=10^{-3}$. We used 100 grid points in the radial direction, 16 in the poloidal direction and 32 in the z direction. The aspect ratio is $R/a=1$, which is not realistic, indeed typical values of the aspect ratio for RFP configurations are about 4. On the other hand, using high values of the aspect ratio implies the use of a larger axial wavenumber spectrum, since the unstable mode

$(1,-2)$ for $R/a=1$ is transposed to the $(1,-8)$ mode for $R/a=4$. For this reason this choice has also been adopted in this paper [4].

The energy of the Fourier harmonic $m=1$, $n=-2$, which is excited by the initial conditions, grows with time and nonlinear interactions transfer energy to smaller wavelengths. After $t=100$ the energy is transferred to the shortest wavelengths allowed by our resolution, and the spectrum of magnetic energy at $t=100$ is shown in Fig. 2. The evolution is characterized by the growth of the unstable mode $(-1,2)$ and its harmonics. The effect of these modes is the reversal of the mean toroidal field, and the final state is dominated by a single helicity, as it was found in [4].

In Fig. 3 the temporal evolution of the field reversal parameter is shown. Initially the configuration loses the reversal very quickly, but, owing to the action of the unstable modes, it is restored after $t \simeq 50$.

Fig. 4 shows the toroidal mean magnetic field $B_z^{0,0}$ as a function of r at $t=100$, which is reversed at the boundary.

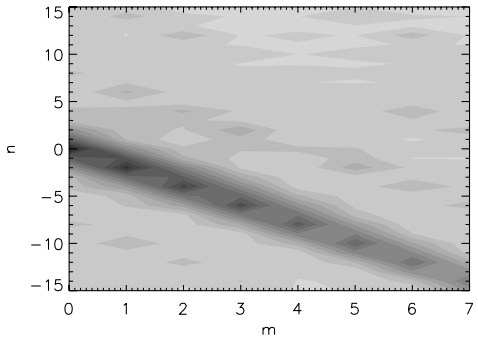

Fig. 2. Magnetic energy spectrum at $t=100$ for Run 1.

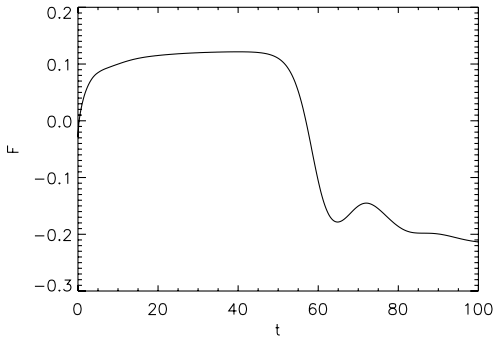

Fig. 3. Temporal evolution of the reversal parameter for Run 1.

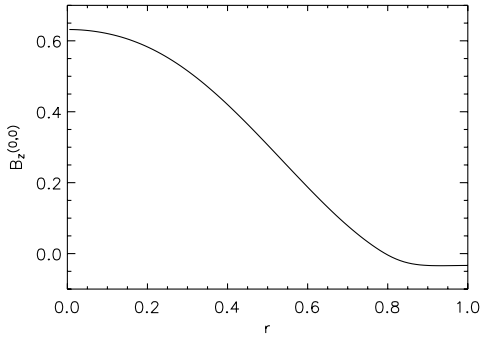

Fig. 4. Toroidal component $B_z^{0,0}$ of the magnetic field at $t=100$ for Run 1.

In the second run (Run 2), we tried to solve the full set of compressible equations, using the same perturbations and aspect ratio that have been used in the previous case, normalized viscosity and resistivity $\mu = \eta = 2 \times 10^{-4}$, $N_r = 128$, $N_\theta = 32$, $N_\phi = 64$. The results obtained from this simulation show that no reversal is obtained. Contrary to what happened in the previous case, the radial velocity is not directed inward, but it brings the plasma towards the boundary and the density decreases in the center. This must be due to the excessive heat of the plasma in the core, produced by the low Reynolds numbers, which overcomes the dynamo effect (Fig. 5).

Realistic values of the Reynolds numbers cannot be used in the numerical simulation due to the high resolution and computational time that would be necessary. Using lower Reynolds numbers we can still describe correctly the energy cascade up to the dissipation scale, but with a shorter energy spectrum. In an incompressible plasma, this prevents to simulate correctly only the phenomena that happen at small scales. On the contrary, in a compressible plasma, the use of low Reynolds numbers may also affect the dynamics of the system at large scales, since the evolution of the pressure is connected with the heating produced at small scales. To avoid this problem, in a third run (Run 3), we eliminated this unrealistic heating, by replacing Eq. (4) with the adiabatic condition $p\rho^{-\gamma} = \text{const}$. In fact, if the thermal conductivity k_t is vanishing, eliminating the viscous and resistive terms, Eq. (4) reduces to:

$$\frac{\partial p}{\partial t} = -\nabla \cdot (\mathbf{v}p) - (\gamma - 1)p\nabla \cdot \mathbf{v}. \tag{24}$$

Using Eq. (1), $\nabla \cdot \mathbf{v}$ can be eliminated in Eq. (24), which can be solved to give the adiabatic condition $p\rho^{-\gamma} = \text{const}$. In this case the plasma density increases in the center, as shown in Fig. 6. Therefore, the inclusion of compressibility drastically changes the long term time evolution of the system, with respect to the case when $p = 0$ and $\rho = \text{const}$. Again the reversal of the magnetic field is quickly lost and then restored after $t \simeq 70$, but, contrary to what has been observed in [4], the reversal parameter changes sign several times (Fig. 7).

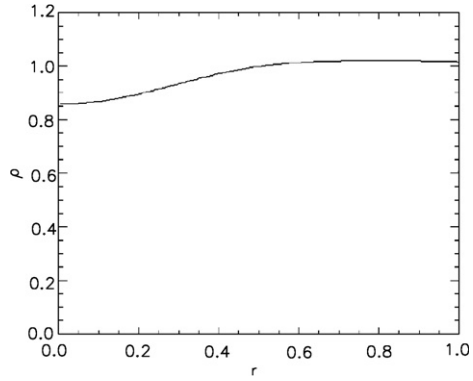

Fig. 5. Radial profiles of density at $t = 100$ for Run 2.

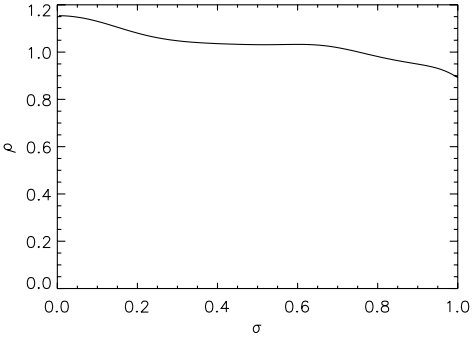

Fig. 6. Radial profiles of density $\rho^{(0,0)}$ at $t = 100$ in the adiabatic case (Run 3).

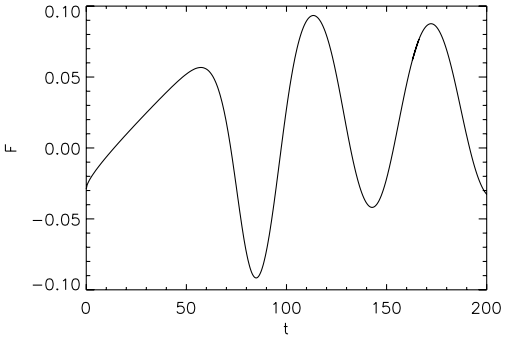

Fig. 7. Time evolution of the reversal parameter in the compressible adiabatic case (Run 3).

7. Conclusions

We developed a numerical code to solve the compressible MHD equations in cylindrical geometry and we used it to study the time evolution of a reversed field pinch configuration. In previous studies of this problem [4], the pressure has been assumed to vanish and the density to be constant and spatially uniform. Such an approach is simpler than to use the full set of MHD equations and it has the advantage of describing physical effects, such as field reversal, actually observed in the RFP devices. However, it is intrinsically not consistent: constant and uniform density requires a divergenceless velocity field, but this latter condition is not necessarily fulfilled when $p = 0$ (cold plasma). In particular, we verified that in such a case $\nabla \cdot \mathbf{v} \neq 0$, which produces a density increase around the axis, in contrast with the assumption of constant and uniform ρ. This inconsistency could affect the time evolution of the system as predicted by the numerical model.

The only way to overcome this problem is to properly describe compressibility, by including both the continuity equation and the equation for the pressure in the numerical model. This represents the main motivation of the present paper. We followed the latter approach, which is more complex than the former one for different reasons: first, the compressible model has two more variables (ρ and p) and two more equations to be solved. The second difficulty concerns the treatment of boundary conditions, which is more complex due to the presence of magnetosonic fluctuations (not present in the other model) which can propagate across the magnetic field, thus connecting the plasma inside the spatial domain with the outside. The complexity of the boundary conditions treatment is enhanced by the cylindrical or toroidal geometry. We used a characteristic decomposition method. Such a method has been applied in the past for hydrodynamics equations in Cartesian geometry [3]. Here we derived characteristic boundary conditions for the MHD equations in cylindrical geometry, in the case of a rigid, conductive wall.

After checking the energy conservation, we tested the code by simulating a zero-pressure plasma with constant density. In that case it has been shown ([5,4]) that the dynamo effect acts so as to sustain the field reversal against resistive diffusion. Our code succeeds in reproducing these results. After that, we considered the compressible case, first using an energy equation which includes viscous and resistive sources and then with an adiabatic energy equation to avoid the eccessive heating coming from the high values of the viscosity and resistivity used in the simulations. In the latter case the field reversal actually takes place, but the time evolution is again different from that derived for $p = 0$ and $\rho = \text{const}$.

In conclusion, our calculation shows the importance of a fully compressible MHD cylindrical code: including compressibility in the RFP configuration not only eliminates an inconsistency of previous models, but it modifies the time evolution derived from the model. Such points should be taken into account in numerical modelling of RFP devices.

Appendix A

The calculation is made here for the cylindrical geometry, but can be extended to the toroidal case. The metric tensor in cylindrical geometry is:

$$g_{ij} = \begin{pmatrix} 1 & 0 & 0 \\ 0 & r^2 & 0 \\ 0 & 0 & 1 \end{pmatrix}$$

and the covariant components of a generic vector **A** are:

$$A_1 = A_r,$$
$$A_2 = rA_\theta,$$
$$A_3 = A_z.$$

Calculating the spatial derivatives in Eqs. (1)–(5) using the covariant components of the vectors, the LODI equations, without the source terms, are:

$$\frac{\partial \rho}{\partial t} + \rho \frac{\partial v_r}{\partial r} + v_r \frac{\partial \rho}{\partial r} = 0, \tag{25}$$
$$\frac{\partial v_r}{\partial t} + v_r \frac{\partial v_r}{\partial r} + \frac{1}{\rho}\frac{\partial p}{\partial r} + \frac{B_z}{\rho}\frac{\partial B_z}{\partial r} + \frac{B_\theta}{r\rho}\frac{\partial (rB_\theta)}{\partial r} = 0, \tag{26}$$
$$\frac{\partial (rv_\theta)}{\partial t} + v_r \frac{\partial (rv_\theta)}{\partial r} - \frac{B_r}{\rho}\frac{\partial (rB_\theta)}{\partial r} = 0, \tag{27}$$
$$\frac{\partial v_z}{\partial t} + v_r \frac{\partial v_z}{\partial r} - \frac{B_r}{\rho}\frac{\partial B_z}{\partial r} = 0, \tag{28}$$
$$\frac{\partial B_r}{\partial t} = 0, \tag{29}$$
$$\frac{\partial (rB_\theta)}{\partial t} + v_r \frac{\partial (rB_\theta)}{\partial r} + rB_\theta \frac{\partial v_r}{\partial r} - B_r \frac{\partial (rv_\theta)}{\partial r} - rv_\theta \frac{\partial B_r}{\partial r} = 0, \tag{30}$$
$$\frac{\partial B_z}{\partial t} + v_r \frac{\partial B_z}{\partial r} + B_z \frac{\partial v_r}{\partial r} - B_r \frac{\partial v_z}{\partial r} - v_z \frac{\partial B_r}{\partial r} = 0, \tag{31}$$
$$\frac{\partial p}{\partial t} + v_r \frac{\partial p}{\partial r} + \gamma p \frac{\partial v_r}{\partial r} = 0. \tag{32}$$

Defining the vector

$$\mathbf{U} = (\rho, v_r, rv_\theta, v_z, B_r, rB_\theta, B_z, p),$$

which contains the covariant components of the vectors **V** and **B**, the LODI set of equations can be cast in the following matrix form

$$\frac{\partial U_\alpha}{\partial t} + A_{\alpha\beta}\frac{\partial U_\beta}{\partial r} = 0,$$

where Greek indices vary in the range $\{1,\ldots,8\}$ and $\{A_{\alpha\beta}\}$ are the elements of the following matrix:

$$A = \begin{pmatrix} v_r & \rho & 0 & 0 & 0 & 0 & 0 & 0 \\ 0 & v_r & 0 & 0 & 0 & \frac{B_\theta}{r\rho} & \frac{B_z}{\rho} & \frac{1}{\rho} \\ 0 & 0 & v_r & 0 & 0 & -\frac{B_r}{\rho} & 0 & 0 \\ 0 & 0 & 0 & v_r & 0 & 0 & -\frac{B_r}{\rho} & 0 \\ 0 & 0 & 0 & 0 & 0 & 0 & 0 & 0 \\ 0 & rB_\theta & -B_r & 0 & -rv_\theta & v_r & 0 & 0 \\ 0 & B_z & 0 & -B_r & -v_z & 0 & v_r & 0 \\ 0 & \gamma p & 0 & 0 & 0 & 0 & 0 & v_r \end{pmatrix}.$$

The velocities of the waves propagating in the radial direction are the eigenvalues $\{\lambda_1,\ldots,\lambda_8\}$ of the matrix A:

$$\lambda_1 = 0, \quad \lambda_2 = v_r, \quad \lambda_3 = v_r - c_{\mathrm{A}r}, \quad \lambda_4 = v_r + c_{\mathrm{A}r},$$
$$\lambda_5 = v_r - c_{\mathrm{s}}, \quad \lambda_6 = v_r + c_{\mathrm{s}}, \quad \lambda_7 = v_r - c_{\mathrm{f}}, \quad \lambda_8 = v_r + c_{\mathrm{f}}$$

with the following definitions:

$$c_{\mathrm{A}r} = \frac{B_r}{\sqrt{\rho}}, \quad c_T^2 = \frac{\gamma p}{\rho},$$
$$c_{\mathrm{s}} = \frac{1}{\sqrt{2}}\sqrt{c_{\mathrm{A}}^2 + c_T^2 - \sqrt{\left(c_{\mathrm{A}}^2 + c_T^2\right)^2 - 4c_T^2 c_{\mathrm{A}r}^2}},$$
$$c_{\mathrm{f}} = \frac{1}{\sqrt{2}}\sqrt{c_{\mathrm{A}}^2 + c_T^2 + \sqrt{\left(c_{\mathrm{A}}^2 + c_T^2\right)^2 - 4c_T^2 c_{\mathrm{A}r}^2}},$$
$$c_{\mathrm{A}}^2 = \frac{B_r^2 + B_\theta^2 + B_z^2}{\rho},$$

c_{A} is the Alfvén velocity, c_{s} and c_{f} are the velocities of slow and fast magnetosonic waves, respectively, Å is the sound speed and $c_{A\mathrm{r}}$ is the Alfvén velocity in the r direction. The eight eigenvalues correspond to eight independent eigenvectors

$$\mathbf{V}_1 = \begin{pmatrix} \frac{1}{c_T^2} \\ -\frac{v_r}{\rho c_T^2} \\ -rB_r \frac{B_r^2(\gamma p - \rho v_r^2)v_\theta + \rho v_r^2(-B_r^2 v_\theta - \gamma p v_\theta + \rho v_r^2 v_\theta + B_\theta B_z v_z)}{\gamma p \rho v_r (B_r^2 - \rho v_r^2)(B_\theta v_\theta + B_z v_z)} \\ B_r \frac{(B_r^2 - \rho v_r^2)(\rho v_r^2 - \gamma p)v_z - B_\theta B_z \rho v_r^2 v_\theta + B_\theta^2 \rho v_r^2 v_z}{\gamma p \rho v_r (B_r^2 - \rho v_r^2)(B_\theta v_\theta + B_z v_z)} \\ \frac{B_r^2(\gamma p - \rho v_r^2) + \rho v_r^2(\rho v_r^2 - \gamma p - B_\theta^2 - B_z^2)}{\gamma p \rho v_r (B_\theta v_\theta + B_z v_z)} \\ r\frac{B_r^2(\rho v_r^2 - \gamma p)v_\theta + \rho v_r^2(B_r^2 v_\theta + \gamma p v_\theta - \rho v_r^2 v_\theta - B_\theta B_z v_z)}{\gamma p (B_r^2 - \rho v_r^2)(B_\theta v_\theta + B_z v_z)} \\ \frac{(B_r^2 - \rho v_r^2)(\rho v_r^2 - \gamma p)v_z - B_\theta B_z \rho v_r^2 v_\theta + B_\theta^2 \rho v_r^2 v_z}{\gamma p (B_r^2 - \rho v_r^2)(B_\theta v_\theta + B_z v_z)} \\ 1 \end{pmatrix},$$

$$\mathbf{V}_2 = (1, \quad 0, \quad 0, \quad 0, \quad 0, \quad 0, \quad 0, \quad 0),$$

$$\mathbf{V}_3 = \left(0, \quad 0, \quad \frac{-rB_z}{B_\theta\sqrt{\rho}}, \quad \frac{1}{\sqrt{\rho}}, \quad 0, \quad \frac{-rB_z}{B_\theta}, \quad 1, \quad 0\right),$$

$$\mathbf{V}_4 = \left(0, \quad 0, \quad \frac{rB_z}{B_\theta\sqrt{\rho}} \quad -\frac{1}{\sqrt{\rho}}, \quad 0, \quad -\frac{rB_z}{B_\theta}, \quad 1, \quad 0\right),$$

$$\mathbf{V}_5 = \left(\frac{1}{c_T^2}, \quad -\frac{c_{\mathrm{s}}}{\gamma p}, \quad \frac{rc_{\mathrm{s}}B_r B_\theta}{\rho\gamma p(c_{\mathrm{s}}^2 - c_{\mathrm{A}r}^2)}, \quad \frac{c_{\mathrm{s}}B_r B_z}{\rho\gamma p(c_{\mathrm{s}}^2 - c_{\mathrm{A}r}^2)}, \quad 0, \quad \frac{rc_{\mathrm{s}}^2 B_\theta}{\gamma p(c_{\mathrm{s}}^2 - c_{\mathrm{A}r}^2)}, \quad \frac{c_{\mathrm{s}}^2 B_z}{\gamma p(c_{\mathrm{s}}^2 - c_{\mathrm{A}r}^2)}, \quad 1\right),$$

$$\mathbf{V}_6 = \left(\frac{1}{c_T^2}, \quad \frac{c_{\mathrm{s}}}{\gamma p}, \quad -\frac{rc_{\mathrm{s}}B_r B_\theta}{\rho\gamma p(c_{\mathrm{s}}^2 - c_{\mathrm{A}r}^2)}, \quad -\frac{c_{\mathrm{s}}B_r B_z}{\rho\gamma p(c_{\mathrm{s}}^2 - c_{\mathrm{A}r}^2)}, \quad 0, \quad \frac{rc_{\mathrm{s}}^2 B_\theta}{\gamma p(c_{\mathrm{s}}^2 - c_{\mathrm{A}r}^2)}, \quad \frac{c_{\mathrm{s}}^2 B_z}{\gamma p(c_{\mathrm{s}}^2 - c_{\mathrm{A}r}^2)}, \quad 1\right),$$

$$\mathbf{V}_7 = \left(\frac{1}{c_T^2}, \quad -\frac{c_{\mathrm{f}}}{\gamma p}, \quad \frac{rc_{\mathrm{f}}B_r B_\theta}{\rho\gamma p(c_{\mathrm{f}}^2 - c_{\mathrm{A}r}^2)}, \quad \frac{c_{\mathrm{f}}B_r B_z}{\rho\gamma p(c_{\mathrm{f}}^2 - c_{\mathrm{A}r}^2)}, \quad 0, \quad \frac{rc_{\mathrm{f}}^2 B_\theta}{\gamma p(c_{\mathrm{f}}^2 - c_{\mathrm{A}r}^2)}, \quad \frac{c_{\mathrm{f}}^2 B_z}{\gamma p(c_{\mathrm{f}}^2 - c_{\mathrm{A}r}^2)}, \quad 1\right),$$

$$\mathbf{V}_8 = \left(\frac{1}{c_T^2}, \quad \frac{c_{\mathrm{f}}}{\gamma p}, \quad -\frac{rc_{\mathrm{f}}B_r B_\theta}{\rho\gamma p(c_{\mathrm{f}}^2 - c_{\mathrm{A}r}^2)}, \quad -\frac{c_{\mathrm{f}}B_r B_z}{\rho\gamma p(c_{\mathrm{f}}^2 - c_{\mathrm{A}r}^2)}, \quad 0, \quad \frac{rc_{\mathrm{f}}^2 B_\theta}{\gamma p(c_{\mathrm{f}}^2 - c_{\mathrm{A}r}^2)}, \quad \frac{c_{\mathrm{f}}^2 B_z}{\gamma p(c_{\mathrm{f}}^2 - c_{\mathrm{A}r}^2)}, \quad 1\right).$$

The radial derivatives can be expressed as a linear combination of the eigenvectors $\{\mathbf{V}_1, \ldots, \mathbf{V}_8\}$ with coefficients, respectively: $\{L_1, L_2, L_{\mathrm{A}r}^-, L_{\mathrm{A}r}^+, L_{\mathrm{s}}^-, L_{\mathrm{s}}^+, L_{\mathrm{f}}^-, L_{\mathrm{f}}^+\}$:

$$\frac{\partial \mathbf{U}}{\partial r} = L_1\mathbf{V}_1 + L_2\mathbf{V}_2 + L_{\mathrm{A}r}^-\mathbf{V}_3 + L_{\mathrm{A}r}^+\mathbf{V}_4 + L_{\mathrm{s}}^-\mathbf{V}_5 + L_{\mathrm{s}}^+\mathbf{V}_6 + L_{\mathrm{f}}^-\mathbf{V}_7 + L_{\mathrm{f}}^+\mathbf{V}_8,$$
$$\frac{\partial \rho}{\partial r} = L_2 + \frac{1}{c_T^2}(L_{\mathrm{s}}^+ + L_{\mathrm{s}}^- + L_{\mathrm{f}}^+ + L_{\mathrm{f}}^- + L_1), \tag{33}$$

$$\frac{\partial v_r}{\partial r} = \frac{c_s}{\gamma p}(L_s^+ - L_s^-) + \frac{c_f}{\gamma p}(L_f^+ - L_f^-) - \frac{v_r}{\rho c_T^2} L_1, \tag{34}$$

$$\frac{\partial (r v_\theta)}{\partial r} = \frac{r B_z}{B_\theta \sqrt{\rho}}(L_{Ar}^- - L_{Ar}^+) + \frac{r c_s B_r B_\theta}{\rho \gamma p (c_s^2 - c_{ar}^2)}(L_s^- - L_s^+) + \frac{r c_f B_r B_\theta}{\rho \gamma p (c_f^2 - c_{ar}^2)}(L_f^- - L_f^+) + S_3 L_1, \tag{35}$$

$$\frac{\partial v_z}{\partial r} = \frac{1}{\sqrt{\rho}}(L_{Ar}^- - L_{Ar}^+) + \frac{c_s B_r B_z}{\rho \gamma p (c_s^2 - c_{ar}^2)}(L_s^- - L_s^+) + \frac{c_f B_r B_z}{\rho \gamma p (c_f^2 - c_{ar}^2)}(L_f^- - L_f^+) + S_4 L_1, \tag{36}$$

$$\frac{\partial B_r}{\partial r} = S_5 L_1, \tag{37}$$

$$\frac{\partial (r B_\theta)}{\partial r} = -\frac{r B_z}{B_\theta}(L_{Ar}^- + L_{Ar}^+) + \frac{r c_s^2 B_\theta}{\gamma p (c_s^2 - c_{ar}^2)}(L_s^- + L_s^+) + \frac{r c_f^2 B_\theta}{\gamma p (c_f^2 - c_{ar}^2)}(L_f^- + L_f^+) + S_6 L_1, \tag{38}$$

$$\frac{\partial B_z}{\partial r} = (L_{Ar}^- + L_{Ar}^+) + \frac{c_s^2 B_z}{\gamma p (c_s^2 - c_{ar}^2)}(L_s^- + L_s^+) + \frac{c_f^2 B_z}{\gamma p (c_f^2 - c_{ar}^2)}(L_f^- + L_f^+) + S_7 L_1, \tag{39}$$

$$\frac{\partial p}{\partial r} = L_s^- + L_s^+ + L_f^- + L_f^+ + L_1, \tag{40}$$

where the terms: S_i, with $i = 1, \ldots, 8$ are the ith components of the eigenvector $\mathbf{V}_1$, respectively.

If we substitute the radial derivatives into the system (25)–(32), then we can write the equations at the boundary with the conditions $v_r = v_\theta = v_z = B_r = 0$ (10)–(14).

References

[1] D. Biskamp, Nonlinear Magnetohydrodynamics, Cambridge University Press, Cambridge, 1997.
[2] P. Martin, Plasma Phys. Control. Fusion 41 (1999) A247.
[3] T.J. Poinsot, S.K. Lele, J. Comput. Phys. 101 (1992) 104.
[4] D. Merlin, D. Biskamp, Numerical studies of MHD turbulence in the reversed field pinch, Report IPP 6/276, Max-Planck-Institut für Plasmaphysik, Garching, 1988.
[5] S. Cappello, D. Biskamp, Nucl. Fusion 36 (1996) 5.
[6] S. Cappello, D. Bonfiglio, D.F. Escande, Phys. Plasmas 13 (2006) 056102.
[7] G. Spizzo, S. Cappello, A. Cravotta, D.F. Escande, I. Predebon, L. Marrelli, P. Martin, R.B. White, Phys. Rev. Lett. 96 (2006) 025001.
[8] S.K. Lele, J. Comput. Phys. 103 (1992) 16.
[9] V.G. Priymak, J. Comput. Phys. 118 (1995) 366.
[10] N. Okong'o, J. Bellan, J. Comput. Phys. 176 (2002) 330.
[11] P.M. Gresho, Annu. Rev. Fluid Mech. 23 (1991) 413.
[12] J.A. Rossmanith, D.S. Bale, R.J. LeVeque, J. Comput. Phys. 199 (2004) 631.
[13] k.W. Thompson, J. Comput. Phys. 68 (1987) 1.
[14] S. Ortolani, D.D. Schnack, Magnetohydrodynamics of Plasma Relaxation, World Scientific, Singapore, 1993.
[15] E.J. Camarana, R.A. Nebel, D.D. Schnack, Phys. Fluids 26 (1983) 1305.
[16] T. Sato, K. Kusano, Phys. Rev. Lett. 54 (1985) 808.
[17] I.H. Hutchinson, Plasma Phys. Control. Fusion 26 (1984) 539.
[18] S. Cappello, R. Paccagnella, Phys. Fluids B 4 (1992) 661.
[19] J.M. Finn, R.A. Nebel, C. Bathke, Phys. Fluids B 4 (1992) 1262.
[20] S. Cappello, D.F. Escande, Phys. Rev. Lett. 85 (2000) 3838.
[21] D.D. Schnack, S. Ortolani, Plasma Phys. 25 (1983) 799.
[22] K. Kusano, T. Sato, Nucl. Fusion 30 (1990) 2075.
[23] Y.L. Ho, C.G. Craddock, Phys. Fluids B 3 (1991) 721.
[24] J.B. Taylor, Phys. Rev. Lett. 30 (1974) 139.
[25] D.D. Schnack, J. Comput. Phys. 70 (1987) 330.
[26] D.C. Robinson, Nucl. Fusion 18 (1978) 939.